Journal of Advanced Research (2012) 3, 295–304

Cairo University

Journal of Advanced Research

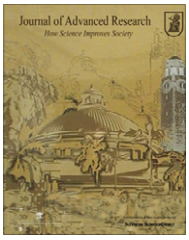

REVIEW ARTICLE

Modeling the deposition of bioaerosols with variable size and shape in the human respiratory tract – A review

R. Sturm *

Brunnleitenweg 41, 5061 Elsbethen, Salzburg, Austria

Received 15 April 2011; revised 30 August 2011; accepted 30 August 2011
Available online 10 October 2011

KEYWORDS

Biogenic particles;
Lung deposition;
Deposition force;
Probabilistic lung model;
Lung disease

Abstract The behavior of bioaerosol particles with various size and shape in the human respiratory tract was simulated by using a probabilistic model of the lung and an almost realistic mathematical approach to particle deposition. Results obtained from the theoretical computations clearly show that biogenic particle deposition in different lung compartments does not only depend on physical particle properties, but also on breathing mode (nose or mouth breathing) and inhalative flow rate (= tidal volume × breathing frequency/30). Whilst ultrafine (< 100 nm) and large (> 5 μm) particles tend to accumulate in the extrathoracic region and the uppermost airways of the tracheobronchial tree, particles with intermediate size are characterized by higher penetration depth, leading to their possible accumulation in the lung alveoli. Due to their deposition in deep lung regions and insufficient clearance, some bioaerosol particles may induce severe lung diseases ranging from infections, allergies, and toxic reactions to cancer.

Characteristics and respiratory uptake of bioaerosols – a brief introduction

In general, the term 'bioaerosol' includes all solid and liquid particles of biological origin that are distributed in the ambient atmosphere. Basically, a bioaerosol may be composed of components emanating from plants (e.g. pollen, endospores, leaf fragments) or animals (e.g. hairs, feathers, droplets of diverse body fluids), but may also contain high abundances of microorganisms. Such microbes occurring in the ambient air among other include bacteria (e.g. *Legionella*, *Actinomycetes*), fungi (e.g. *Histoplasma*, *Alternaria*, *Penicillium*, *Aspergillus*), protozoa (e.g. *Naegleria*, *Acanthamoeba*), viruses (e.g. *Influenza*), and algae (e.g. *Chlorococcus*) [1–3]. An essential source of bioaerosols, which is not mentioned very frequently, comprises industries manufacturing biogenic substances (e.g. wood or cotton industry). Due to the mechanical treatment of the organic raw materials, certain amounts of related dust particles are emitted to the atmosphere, where they may represent significant environmental burdens [4].

Concerning their sizes and shapes, bioaerosols are commonly characterized by high variability. Whilst viruses are usually smaller than 0.2 μm, bacteria, spores, and fungal cells vary

* Corresponding author. Tel.: +43 662 633321; fax: +43 662 8044 150.
E-mail address: Robert.Sturm@sbg.ac.at

Peer review under responsibility of Cairo University.
doi:10.1016/j.jare.2011.08.003

ELSEVIER Production and hosting by Elsevier

in size between 0.25 μm and 60 μm. Diameters of pollen originating from various gymno- and angiosperms range from 5 μm to 300 μm, whereas small arthropods (e.g. dust mites) transported through the atmosphere and thus subsumed under the term 'aero-plankton' may reach sizes up to 1 mm. Most significant variations in size may be attested to airborne cell fragments and cell colonies, ranging from several nanometers to hundreds of micrometers [5,6]. Shapes of bioaerosol particles may be attributed to three basic categories: Besides particles with perfectly (liquid droplets) or approximately spherical shapes (spores, coccal bacteria, some pollen), also particles with rod- or fiber-like geometries (bacilli, hairs) and particles with disk- or platelet-like geometries (dusts, plant fragments) may be distinguished with the help of advanced optical techniques [1].

An important aspect concerns the hygienic relevance of bioaerosol particles. Whilst numerous pathogenic microorganisms, when inhaled from the ambient air, may cause infectious insufficiencies such as Legionnaire's disease or Pontiac fever, other constituents of bioaerosols may be responsible for hypersensitivity or allergic diseases like asthma, allergic rhinitis, extrinsic allergic alveolitis or humidifier fever [7,8]. Another type of bioaerosol-induced insufficiencies are toxic reactions that are evoked by the inhalation of toxic substances of natural origin (e.g. β-1,3-glucans, mycotoxins) [9,10]. As underlined by numerous medical studies [9–11], chronic exposure to endotoxins (bacterial origin) or mycotoxins (fungal origin) may among other lead to bronchitis, asthma and organic dust toxic syndrome (ODTS) or toxic alveolitis.

In order to appropriately study the behavior and possible hygienic effects of bioaerosol particles in the human respiratory tract (HRT), knowledge of their deposition in single compartments of the lungs and specific airways of a given lung generation has to be regarded as indispensable. Since the experimental approach of pulmonary bioaerosol deposition fails due to the hazardous effects of many biogenic particles, theoretical computations based on reliable models of particle transport and deposition within almost realistic lung structures may help to elevate this level of information. In the review presented here deposition of variably sized and shaped biogenic particles is theoretically calculated under the assumption of different breathing modes (nasal and oral inhalation) and breathing scenarios (sitting, light-work, and heavy-work breathing).

Computation of bioaerosol deposition in the human lungs

Basic features of the mathematical model

Current mathematical approaches to aerosol particle deposition in the HRT are founded upon an airway architecture consisting of numerous sequences of straight cylindrical tubes that form a tree-like structure [12,13]. Contrary to early morphometric models, which have assumed the branching network to correspond to a completely symmetric tree structure with uniform path lengths from the trachea to the closing alveolar sacs [12], actual morphometric approaches more appropriately account for intrasubject variability of airway geometry in specific lung generations. This is mainly realized by the application of asymmetric models of the lung structure, where geometric variations of single airway segments in a given lung generation are based on statistical computations of morphometric data sets [14,15]. Most currently, asymmetry and randomness of the branching airway system are expressed by the use of a stochastic model of the human tracheobronchial tree [16], with geometric parameters (airway length, airway diameter, branching angle of a bifurcation, gravity angle) being randomly selected from probability-density functions that have been derived from related probability distributions [17].

The stochastic approach to particle transport and deposition in the HRT is based on the mathematical principle of random walk of inhaled particles through the airway branching structure generated in the way noted above. At each bifurcation, the decision of the particle to be transported either to the major or to the minor daughter airway is also randomly determined by application of respective air-flow distributions which arise from the hypothesis that flow splitting is proportional to distal volume [18]. As a main feature of stochastic transport and deposition model, computation of particle deposition in a specific airway is regarded to reflect the average deposition behavior of many (e.g. 10,000) particles. This inference from a single deposition event to the entirety of inhaled particles is appropriately supported by the so-called Monte Carlo technique that is subject to a further improvement by application of the statistical weight method [16]. Here, deposition of a particle in a selected airway is simulated by decreasing its statistical weight instead of completely terminating its path. The contribution of an individual deposition event to total deposition in a given airway generation is determined by multiplication of the actual statistical weight of the particle with the site-specific deposition probability.

Concerning the determination of particle deposition fractions in individual airways due to various physical deposition forces, analytical deposition equations are applied which are exclusively valid for straight cylindrical tubes and spherical spaces (Table 1) [19,20]. In addition to the standard formulae, particle deposition by Brownian motion is also simulated by the empirical equation provided by Cohen and Asgharian [21] that considers increased deposition in the upper bronchial airways due to developing flow. For deposition of small particles in more peripheral airway tubes, the diffusion equation proposed by Ingham [22] is additionally applied. Enhanced levels of tracheal particle accumulation caused by turbulent flow (laryngeal jet) are commonly expressed by correction factors that have been included into the respective standard formula for inertial impaction. Regarding the theoretical estimation of extrathoracic deposition efficiencies, indicating the ability of nasal and oral airways to filter inspired particulate material, empirical equations derived from both *in vivo* measurements [23] and collected experimental data [24] have been added to the approach.

For extremely anisometric particles such as long fibers or thin platelets with large diameters, interception has to be regarded as an additional deposition mechanism in the upper tracheobronchial tree. This phenomenon describes the deposition of nonspherical particles at the carinal sites of the bronchial airway bifurcations which is exclusively caused due to the orientation of the particles' main axes perpendicular to the flow direction of the air stream. As outlined in previous publications, where interception of long fibers was approximated numerically [25–27], fibrous particles (and platelets) tend to rotate around their center of gravity rather than being oriented parallel to the air stream, when they are transported

Table 1 Deposition mechanisms and related mathematical equations for the computation of biogenic particle deposition in cylindrical tubes (=airways) and spherical spaces (=alveoli) [19,20,28].

Mechanism	Equation(s), variables	Coefficients
Cylindrical tubes		
Brownian motion	$p_d = 1 - \Sigma\ a_i exp(-b_i x) - a_4 exp(-b_4 x^{2/3})$ $x = LD/2R^2 v$ D...diffusion coefficient R...radius of the tube L...length of the tube v...mean flow velocity	$a_1 = 0.819$, $b_1 = 7.315$ $a_2 = 0.098$, $b_2 = 44.61$ $a_3 = 0.033$, $b_3 = 114.0$ $a_4 = 0.051$, $b_4 = 79.31$
Sedimentation	$p_s = 1 - exp[-(4gC\rho r^2 L\ cos\varphi)/(9\pi\mu R v)]$ g...acceleration of gravity (9.81 m s^{-2}) φ...angle of tube relative to gravity ρ...density of the particle C...Cunningham slip correction factor r...radius of the particle μ...viscosity of the fluid	–
Inertial impaction	$p_i = 1 - (2/\pi)\ cos^{-1}(\Theta St) + (1/\pi)\ sin$ $[2\ cos^{-1}(\Theta St)]\ for\ \Theta St < 1$ $p_i = 1\ for\ \Theta St > 1$ Θ...branching angle St...Stokes number	–
Inertial impaction and interception (only for extremely anisometric particles)	$p_{imp,int} = a\ exp[-exp(b - c\ St)]$ St...Stokes number $St = [\rho(d\beta^{1/3})^2 V]/18\mu D_a$ ρ...density of the particle d...diameter of the particle β...aspect ratio (Table 2) V...mean velocity of the particle μ...dynamic viscosity of air D_a...diameter of the airway	$a = 0.8882$ $b = 1.6529$ $c = 4.7769$
Spherical spaces (uniform distribution of particles in the air, ideal alveolar mixing)		
Brownian motion	$p_d = 1 - (6/\pi^2)\ \Sigma\ (1/n^2)\ exp(-Dn^2\pi^2 t/R^2)$ n runs from 1 to ∞ D...diffusion coefficient t...time R...alveolar radius	–
Sedimentation	$p_s = 0.5(u_s t/2R)\ [3 - (u_s t/2R)^2]\ if\ t < 2R/u_s$ $p_s = 1\ if\ t \geqslant 2R/u_s$ u_s...settling velocity	–

through the bronchial airway net. The pulse for this rotation of the particles during their transport is assumed to partially origin from secondary flows at the airway bifurcations themselves. In order to take account for this essential deposition process, the respective approach of Zhang et al. [28] was used, because in the outlined formula (Table 1) inertial impaction and interception are hypothetized to occur as a combined effect. Basically, consideration of interception was limited to particles with an aspect ratio $\beta \leqslant 0.03$ or $\beta \geqslant 30$ (see below). For these anisometric particulate bodies, impaction was not calculated with the conventional empirical equation but with the approximative formula of Table 1, whereby geometric particle properties were implemented in the Stokes number. Formulae for interception were applied by assuming random particle orientation at each airway bifurcation of the upper tracheobronchial tree.

For transport and deposition calculations, all bronchial airway lengths and diameters are routinely scaled down to a functional residual capacity of 3300 ml. The additional air volume produced by inhalation (tidal volume) does not cause a geometric modification among the bronchial airways, but is fully compensated by an isotropic increase of the alveolar diameter.

Theoretical approach to the transport and deposition of non-spherical particles

Since most bioaerosol particles significantly deviate from ideal spherical shape, except for interception deposition computations introduced in the preceding section are not applicable without any geometry-specific correction. A widely accepted mathematical concept, which exclusively focuses on the shape of airborne particles, is the so-called aerodynamic diameter. Basically, this parameter denotes the diameter of a spherical particle with unit-density (1 g cm^{-3}) that is characterized by exactly the same aerodynamic properties as the non-spherical particle of interest [29–31]. As summarized in Table 2, the aerodynamic diameter, d_{ae}, commonly depends on the volume equivalent diameter, d_{ve}, which represents the diameter of a sphere with identical volume as the bioaerosol particle, the dynamic shape factor, χ, the density of the studied particle, ρ_p, and the Cunningham correction factor quotient $C_c(d_{ve})/$

Table 2 Physical parameters and related mathematical equations, variables and coefficients for the theoretical computation of nonspherical particle transport in the HRT [29–31].

Physical parameter	Equation(s), variables	Coefficients		
Aerodynamic diameter	$d_{ae} = d_{ve}\,[(1/\chi)(\rho_p/\rho_0)(C_c(d_{ve})/C_c(d_{ae}))^{0.5}$ d_{ve}...volume equivalent diameter χ...dynamic shape factor ρ_p...density of particle ρ_0...unit-density (1 g cm^{-3}) $C_c(d_{ae})$...Cunningham slip correction factor for d_{ae} $C_c(d_{ve})$...Cunningham slip correction factor for d_{ve}	–	–	–
Volume equivalentdiameter	$d_{ve} = [(6/\pi)\ V_p]^{(1/3)}$ V_p...volume of non-spherical particle	–	–	–

Dynamic shape factor	$1/\chi = 1/3\chi_{//} + 2/3\chi_{\_\vert\_}$
	$\chi_{//}$...dynamic shape factor for particle movement parallel to the air stream
	$\chi_{\_\vert\_}$...dynamic shape factor for particle movement perpendicular to the air stream
		–	–	–

	$\chi = [(a_1/3)(\beta^2-1)\beta^{-(1/3)}]/[(2\beta^2-a_2)/a_3{}^{0.5}\ F(a_4) + a_5]$	Oblate disks		
			$\chi_{//}$	$\chi_{\_\vert\_}$
		a_1	4	4
		a_2	3	1
		a_3	$1-\beta^2$	$1-\beta^2$
		a_4	β	β
		a_5	β	$-\beta$
		F	arccos	arccos
		Fibers and rods		
			$\chi_{//}$	$\chi_{\_\vert\_}$
		a_1	8	8
		a_2	3	1
		a_3	β^2-1	β^2-1
		a_4	$\beta + (\beta^2-1)^{0,5}$	$\beta + (\beta^2-1)^{0,5}$
		a_5	β	$-\beta$
		F	ln	ln
Aspect ratio	$\beta = l_p/d_p$ l_p...length of particle d_p...geometric diameter of particle	–	–	–
Cunningham slip correction factor	$C_c = 1 + \lambda/d_p\ [2.514 + 0.800\ exp(-0.55 d_p/\lambda)]$ λ...mean free path length of air molecules (0.066 μm at 20 °C)	–	–	–

$C_c(d_{ae})$. Besides the volume equivalent diameter, the most significant parameter for the determination of the aerodynamic diameter is the dynamic shape factor which may be computed according to empirical formulae, chiefly depending on the so-called aspect ratio, β, of the investigated particle (Table 2). This ratio simply denotes the length of the particle divided by its diameter and, thus, takes values >1 for fibers and values <1 for platelets or disks. In order to consider variations of non-spherical particle transport being oriented either parallel or perpendicular to the flow direction of the inhaled air stream, the dynamic shape factor is subdivided into a parallel component, $\chi_{//}$, and a perpendicular component, $\chi_{\_\vert\_}$. As demonstrated in Fig. 1, calculated numbers for χ, $\chi_{//}$, and $\chi_{\_\vert\_}$ take values >1 for $\beta > 1$ and $\beta < 1$, but uniformly amount to 1 in the case of $\beta = 1$ (spheres). The Cunningham correction factors for the aerodynamic diameter, $C_c(d_{ae})$, and the volume equivalent diameter, $C_c(d_{ve})$, are of minor importance in the so-called continuum regime (Knudsen number $K_n \ll 1$) that has to be exclusively regarded as realistic aerodynamic environment for particles with μm-size. Particles with diameters $\ll 1$ μm and especially those approaching the size of molecules (nano-particles) have to be attributed to the so-called slip-flow regime ($K_n \geqslant 1$), where their interaction with air molecules becomes a determinant concerning both their transport and deposition in the HRT. This is mainly expressed by the Cunningham slip correction factors taking values up to 10^4. They are computed by an exponential function, depending on the quotient of the respective particle diameter (d_{ae} or d_{ve}) and the mean free path length of air molecules, λ (0.066 μm at 20 °C, Table 2). After determination of the aerodynamic diameter according to the equations listed in Table 2, empirical and semi-empirical formulae of Table 1 are applicable without any limits to this parameter.

In the contribution presented here, besides the transport and deposition simulation of spherical particles with unit-density ($d_{ae} = d_{ve} = d_g$, where d_g = geometric diameter) also the behavior of platelet- and disk-like particles ($0.01 \leqslant \beta < 1$, $d_{ae} < d_{ve} < d_g$) and fibrous particles ($1 < \beta \leqslant 100$, $d_g < d_{ve} < d_{ae}$) with density ranging from 0.5 g cm^{-3} (plant

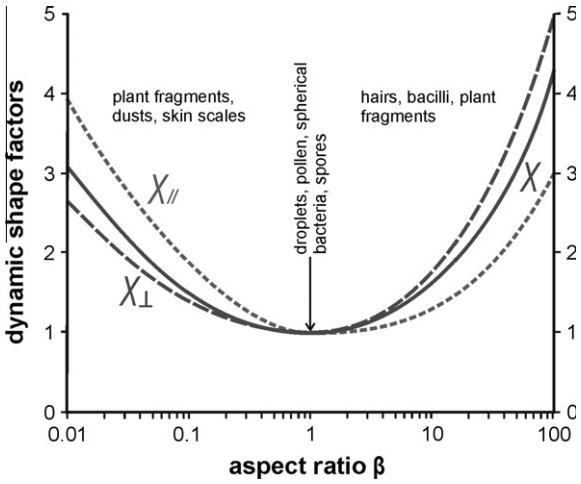

Fig. 1 Dependence of the dynamic shape factors $\chi_{//}$, $\chi_{\perp}$, and χ on the aspect ratio β [30]. As additionally illustrated in the graph, $\beta < 1$ corresponds to disk- or platelet-like particles like plant fragments and dusts, $\beta = 1$ to spherical particles like liquid droplets, pollen or spores, and $\beta > 1$ to fibrous particles such as hairs or bacilli.

fragments) to 1.0 g cm^{-3} (cells) was subjected to a detailed theoretical computation.

Theoretical deposition of bioaerosol particles in the HRT

Total and regional deposition

By definition, total deposition of aerosol particles in the HRT is determined by the quotient between the number or mass of inhaled particles and the number or mass of exhaled particles. Hence, total deposition considers both particle deposition in the extrathoracic region (i.e. oral or nasal pathway) as well as particle accumulation in the thoracic compartment. The thoracic compartment itself may be subdivided into the air-conducting zone, including the bronchi and non-alveolated bronchioles, and the gas-exchange zone including the respiratory (alveolated) bronchioles and the alveolar closing sacs.

Regarding the total deposition graphs proposed in Figs. 2 and 3, a clear deposition force-controlled relationship between the level of total deposition and aerodynamic particle diameter may be observed. Concerning total deposition of bioaerosol particles after inhalation through the nose (Fig. 2), mainly ultrafine particles ($d_{ae} < 0.1$ µm) and large particles ($d_{ae} > 3$ µm) are characterized by deposition fractions approximating 100%. Besides these two maxima also a deposition minimum, being located at $d_{ae} \approx 0.5$ µm, may be recognized which commonly takes values between 20% and 30%. Differences of breathing frequency and tidal volume arising between the three breathing conditions (sitting breathing, light-work breathing, heavy-work breathing [32]) are chiefly reflected by the shape of the total deposition graph and the positions of the maxima and the minimum. As unequivocally demonstrated by the graphs of Fig. 2, low inhalative flow rate results in a preferential deposition of ultrafine particles, whilst total deposition of large particles is subject to a measurable decrease. By an elevation of the inhalative flow rate a reversal of the described phenomena

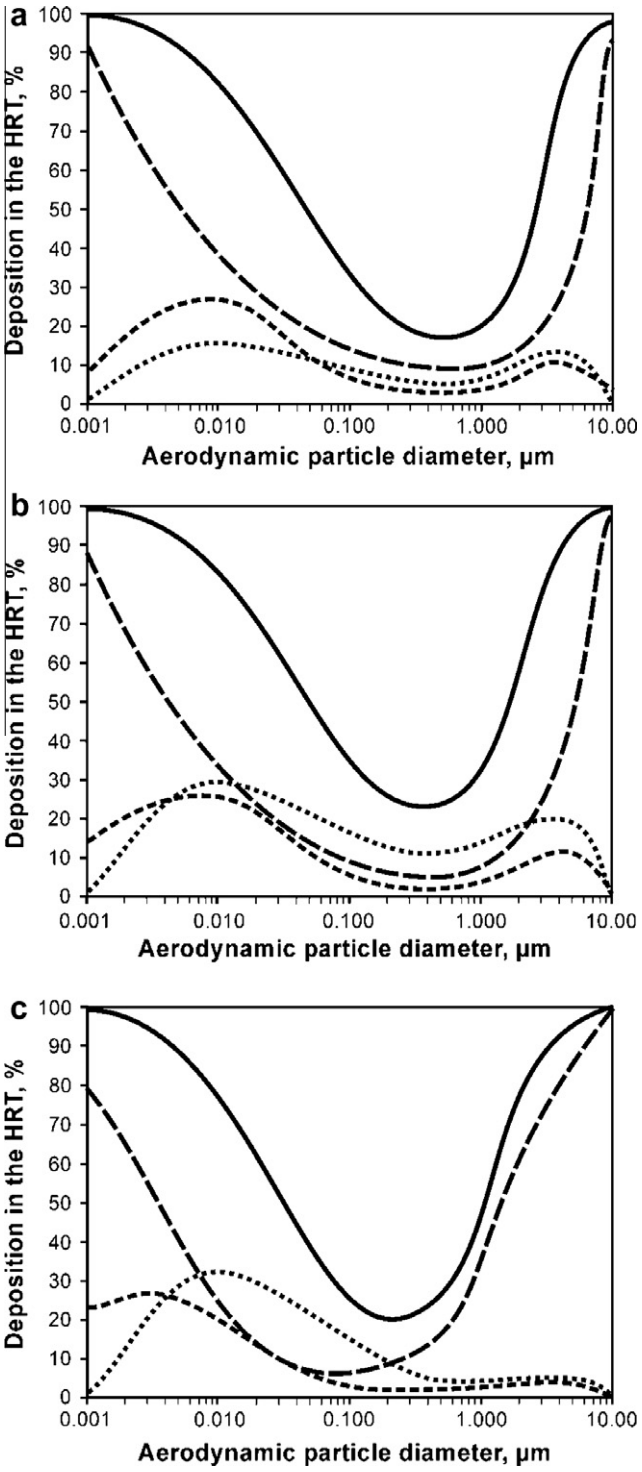

Fig. 2 Total deposition (solid line), extrathoracic deposition (dashed line), bronchial deposition (short-dashed line) and acinar deposition (dotted line) and their dependence on aerodynamic particle diameter after inhalation through the nose: (a) sitting breathing, (b) light-work breathing, (c) heavy-work breathing.

(i.e. slight decrease of ultrafine particle deposition, increase of large particle deposition) may be observed. A change from nasal inhalation to inhalation through the mouth has two significant consequences for total deposition of

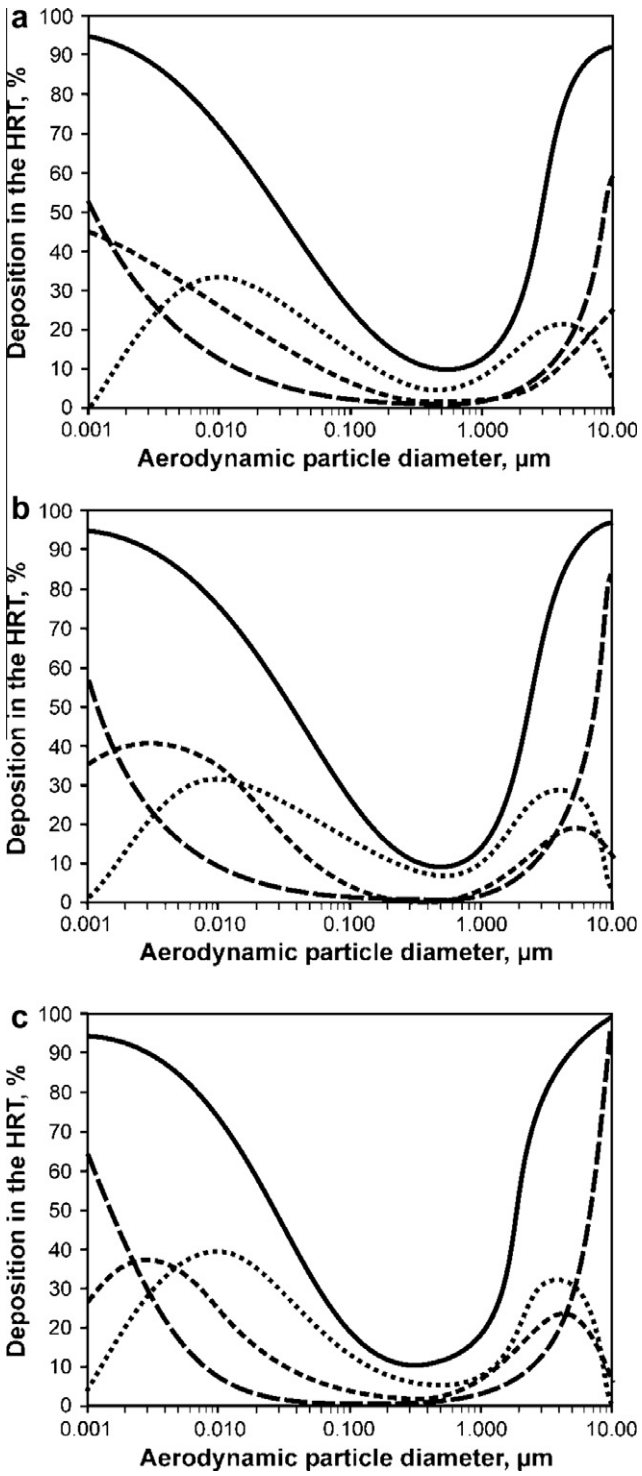

Fig. 3 Total deposition (solid line), extrathoracic deposition (dashed line), bronchial deposition (short-dashed line) and acinar deposition (dotted line) and their dependence on aerodynamic particle diameter after inhalation through the mouth: (a) sitting breathing, (b) light-work breathing, (c) heavy-work breathing.

bioaerosol particles: First, deposition maxima of ultrafine and large particles generally take lower values with respect to those generated after nasal inhalation; second, the deposition minimum occurring at intermediate particle sizes is also subject to a remarkable decrease, thereby not exceeding 17%.

Regional (i.e. extrathoracic, bronchial, and acinar) deposition is characterized by a significant dependence on the breathing mode (Figs. 2 and 3). Regarding inhalation through the nose, highest fraction of particles with $d_{ae} < 0.01$ µm and $d_{ae} > 5$ µm is already accumulated in the extrathoracic region (nose, nasopharynx, and larynx). Similar to the theoretical curves computed for total deposition, extrathoracic particle accumulation is marked by two maxima (ultrafine and large particles) and a minimum occurring at intermediate values for d_{ae} (0.05–1 µm). Any change of the breathing conditions is accompanied by respective translocations of the maxima and the minimum along the two coordinate axes and a modification of the curve shape (Fig. 2). Due to the filtering effect in the extrathoracic airways, deposition of bioaerosol particles in the bronchi and non-alveolated bronchioles takes lower values (3–28%), whereby again very small (ca. 0.01 µm) as well as large particles (ca. 3 µm) show a preference to be deposited in the air-conducting zone of the HRT. With increasing breathing frequency and inhalative flow rate deposition of ultrafine particles is successively remains constant or is slightly increased, whereas deposition fractions of large particles are subject to a remarkable decrease. Particle deposition in the gas-exchange zone of the HRT may be theoretically described by a bimodal curve, with respective maxima being located at $d_{ae} = 0.01$ µm and $d_{ae} = 3$ µm. Here, change of the breathing conditions has a remarkable effect on the heights of the two peaks (left one becomes higher, right one lower). A switch from nasal to oral breathing is accompanied by several modifications with regard to the deposition behavior of bioaerosol particles (Fig. 5): First, extrathoracic deposition is significantly decreased, taking about 60% of the value obtained after nasal inhalation; second, bronchial and alveolar deposition fractions are characterized by measurable elevations due to the lack of particle filtering in the preceding compartment of the HRT.

Deposition in the airway generations of the HRT

As depicted in the graphs of Figs. 4 and 5, airway generation-specific bioaerosol particle deposition was computed for five different values of d_{ae} (0.001 µm, 0.01 µm, 0.1 µm, 1 µm, and 10 µm), again assuming nasal and oral inhalation as well as three separate conditions of breathing (see above). Deposition fractions in airway generations 0 (trachea) to 25 (outermost respiratory bronchiole) produced after inhalation through the nose (Fig. 4) commonly vary between 0.01% and 6.00%, whereby each particle size class is marked by a highly specific deposition pattern. Whilst 0.001-µm and 10-µm increasingly tend to deposit in the proximal airway generations, 0.01-µm and 0.1-µm particles are preferably accumulated in intermediate to distal airway generations (maxima at generations 15 and 17). Bioaerosol particles with $d_{ae} = 1$ µm is not characterized by a remarkable generation of deposition peaks (maximum at generation 18). By changing the breathing conditions, deposition patterns undergo a partly significant modification in shape, with peak heights of 0.001-µm and 0.01-µm particles being subject to either an increase.

Airway generation-specific deposition of bioaerosol particles after inhalation through the mouth differs from respective deposition produced after nasal inhalation insofar as significantly higher particulate fractions may penetrate to the air-conducting and gas-exchange zone (0.01–7.5%, Fig. 5). Deposition patterns computed for the single particle size

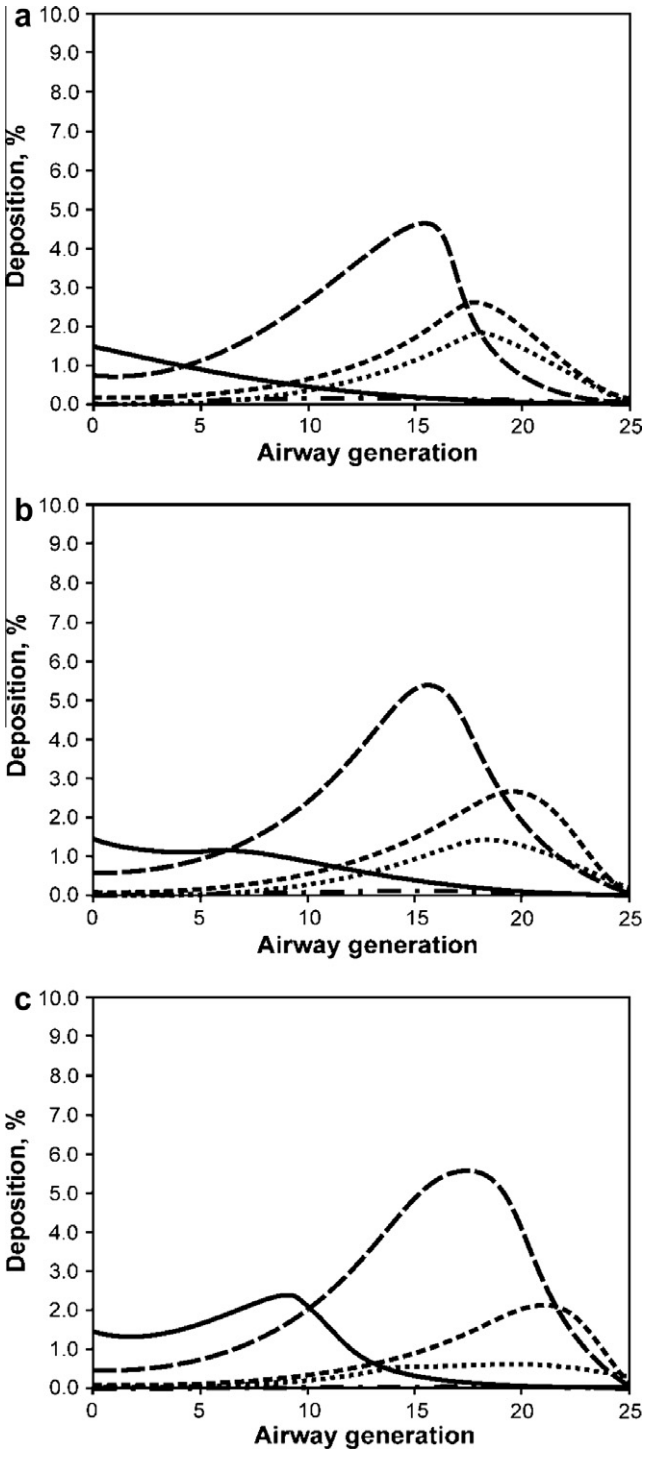

Fig. 4 Generation-by-generation deposition of 0.001-μm particles (solid line), 0.01-μm particles (dashed line), 0.1-μm particles (short-dashed line), 1-μm particles (dotted line), and 10-μm particles (dashed-dotted line) after inhalation through the nose: (a) sitting breathing, (b) light-work breathing, (c) heavy-work breathing.

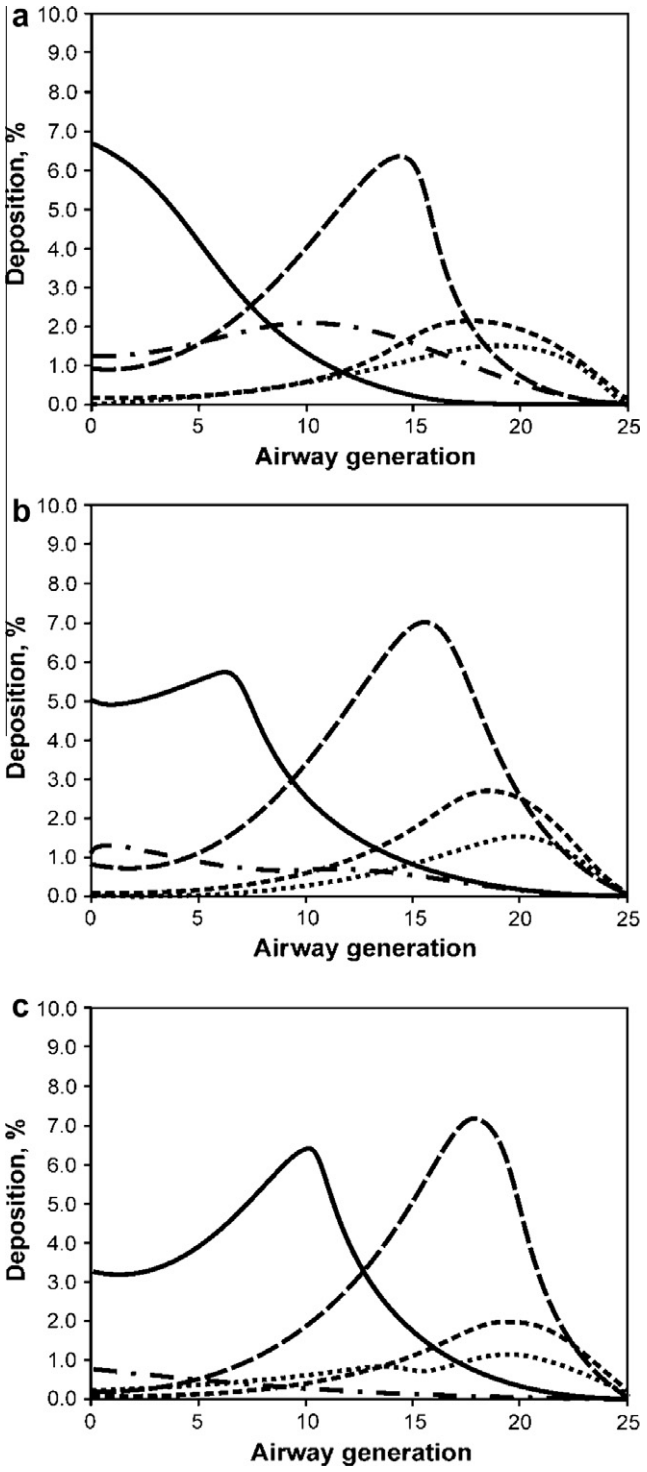

Fig. 5 Generation-by-generation deposition of 0.001-μm particles (solid line), 0.01-μm particles (dashed line), 0.1-μm particles (short-dashed line), 1-μm particles (dotted line), and 10-μm particles (dashed-dotted line) after inhalation through the mouth: (a) sitting breathing, (b) light-work breathing, (c) heavy-work breathing.

classes commonly show the properties regarding peak position similar to those generated for nasal breathing. In accordance with nasal inhalation any increase of the inhalative flow rate results in an intensification of deposition in the case of ultrafine and intermediately sized particles and a weakening of deposition in the case of large particulate matter.

Lung penetrability of diverse bioaerosol particles

An essential question concerning bioaerosol-associated health effects deals with the lung penetrability of biogenic particles under different breathing conditions and under the assumption of nasal and oral inhalation (Fig. 6). Penetration depths (i.e. outermost airway generations being reached by the particles) were computed for particle sizes ranging from 0.001 µm to 10 µm. As clearly exhibited in graphs of Fig. 6, highest penetration depth (airway generation 28) may be attested for particles with d_{ae} = 0.5 µm, whereas particles with d_{ae} = 0.001 µm and d_{ae} = 10 µm are characterized by a rather limited ability to penetrate the lung (airway generations 15 and 18). Whilst the breathing mode has a partly significant effect on the penetration depth of diverse particle size classes, elevation of the inhalative flow rate may influence penetrability by either an increase (< 1 µm) or a decrease (10 µm) of the airway generation number being reached by the inhaled particulate mass.

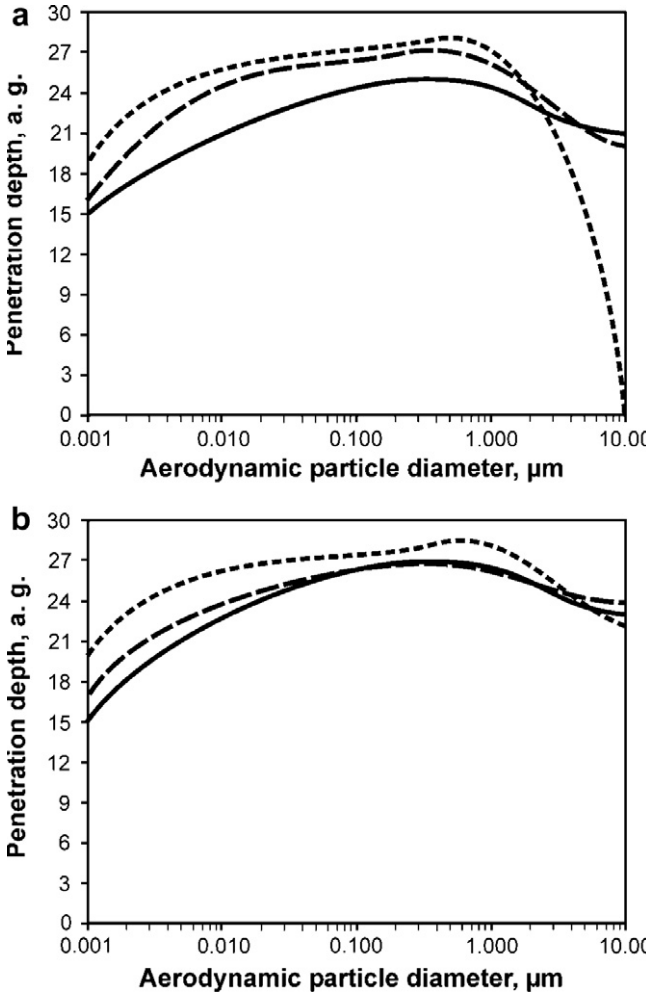

Fig. 6 Penetration depth (deposition > 0.01%) and its dependence on aerodynamic particle diameter (sitting breathing: solid line; light-work breathing: dashed line; heavy-work breathing: dotted line): (a) inhalation through the nose, (b) inhalation through the mouth (a.g. = airway generation).

Factors influencing the deposition of bioaerosols in the human respiratory tract

As unequivocally demonstrated by computer simulations presented in this contribution, biogenic particles with specific size and shape may penetrate to deep lung regions, where they subsequently may unfold their unwholesome efficacy. Main factors disposing of the deposition site of an inhaled particle are the physical characteristics of that particle, causing specific proportionate shares of the four main deposition forces (Brownian motion, inertial impaction, gravitational settling, interception [16,32]), and the breathing conditions existing during inhalative uptake of bioaerosols. Under given breathing conditions, mainly those particles, which due to their aerodynamic diameters offer an insignificant target to deposition forces, are enabled to penetrate to outermost lung generations, where they finally may settle down in the alveoli. As proposed in the graphs of Figs. 2 and 3, such deposition force-insensitive particles generally vary in size between d_{ae} = 0.1 µm and d_{ae} = 1 µm [32,33]. Among those bioaerosols occurring with highest abundances in the ambient air cell fragments, viruses, small bacteria, and small spores have the potency to reach the gas-exchange zone of the HRT, where they may excite allergic reactions or infectious diseases. In certain cases, they may also be responsible for malignant transformations of bronchial/alveolar cells, finally resulting in the generation of lung carcinomas [34].

Similar to dusts, soots, and other particles of the ambient atmosphere, also biogenic particles may lose significant parts of their hazardous potential, if they are inhaled through the nose [23,24,35,36]. Due to the anatomy of the nasal cavity consisting of several flow-splitting conches and the posterior nasopharynx compelling the air stream to execute a 90° turn [32], most of the inhaled particulate mass is already filtered in this extrathoracic compartment (Fig. 7). A completely

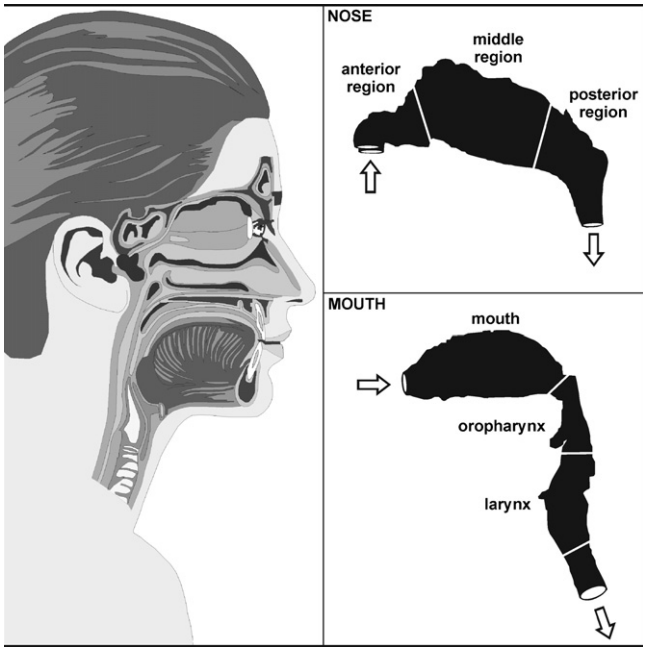

Fig. 7 Morphology of the extrathoracic airways for demonstrating the filtering efficiency of these particle paths.

different situation is given for mouth breathing, where remarkably higher particle fractions are able to overcome the extrathoracic structures (mouth cavity, oropharynx) and to reach the posterior lung airways. The theoretical predictions yielded evidence that the inhalative flow rate (tidal volume × breathing frequency/30) has a remarkable influence on the deposition of biogenic particles in the main compartments of the HRT. Based on the particle deposition formulae summarized in Table 1, the transport velocity of the particle-loaded air positively correlates with the deposition probability due to inertial impaction. On the other side, velocity of the inhaled air stream is characterized by a negative correlation with deposition probabilities arising from both Brownian motion and gravitational settling [32,34]. As a main consequence of this phenomenon, large particles are increasingly deposited in the proximal airway generations, when inhalative flow rate is elevated, whilst higher amounts of small and intermediately sized particles are transported to more distal airways or are exhaled again (Fig. 3–6).

Immediately after their deposition the bioaerosol particles are subjected to the innate defense system of the lung that mainly consists of a fast clearance mechanism, represented by the so-called mucociliary escalator, and several slower clearance mechanisms [32,34,37]. If particles were mainly deposited on the surface liquid layer (mucous layer) of the bronchial airways, their complete removal from the HRT requires several days. Smaller particles have a higher tendency to reach the periciliary spaces beneath the mucous layer and to be subsequently cleared by slower mechanisms such as uptake by airway macrophages or epithelial transcytosis [32,37]. In this case, complete removal of the particulate mass may be on the order of weeks to months. This circumstance, however, offers a chance to the particles to unfold their pathogenic potential. If particles from inhaled bioaerosols are accumulated in the acinar region and especially in the alveoli, their clearance is exclusively determined by time-consuming processes (uptake by alveolar macrophages, transport into the interstitium, etc.). Here, eventual injuries to health become even more evident than in the case of bronchial deposition. Another problem arises, if bioaerosols are taken up by subjects already suffering from chronic lung diseases like chronic bronchitis or chronic asthma. In these cases probabilities of infections (e.g. by inhaled bacteria) or allergic reactions (e.g. by inhaled hairs, plant fragments, etc.) are much more likely [38,4].

Conclusions

It could be concluded that the amount and the site of bioaerosol particle deposition in the HRT are determined by a rather wide spectrum of physical and physiological factors. Specific combinations of particle properties (size, shape, density) with certain breathing conditions may, in one case, result in an almost complete deposition of the particulate mass in the extrathoracic region, but may, in another case, cause a highly effective penetration of the bioaerosol to the gas-exchange region of the HRT. This hazardous potential of bioaerosols, however, requires a respective investigation of air quality at those working places which are preferable targets of bioaerosol release (e.g. cotton spinning mills) or production (e.g. wood processing industries).

References

[1] Burge H. Bioaerosols: prevalence and health effects in the indoor environment. Aller Clin Immunol 1990;86:686–701.
[2] Owen MK, Ensor DS, Sparks LE. Airborne particle sizes and sources found in indoor air. Atmos Environ 1992;26A:2149–62.
[3] Seltzer JM. Biologic contaminants. Occup Med 1995;10:1–25.
[4] Husmann T. Health effects of indoor-air microorganisms. Scand J Work Environ Health 1996;22:5–13.
[5] Nevalainen A, Willeke K, Liebhaber F, Pastuszka J. Bioaerosol sampling. In: Willeke K, Baron PA, editors. Aerosol measurement–principles techniques, and applications. New York: Van Nostrand Reinhold; 1993. p. 471–92.
[6] Neef A, Amann R, Schleifer KH. Detection of microbial cells in aerosols using nucleic acid probes. System Appl Microbiol 1995;18(1):113–22.
[7] Heldal KK, Halstensen AS, Thorn J, Djupesland P, Wouters I, Eduard W, et al. Upper airway inflammation in waste handlers exposed to bioaerosols. Occup Environ Med 2003;60:444–50.
[8] Herr CEW, zur Nieden A, Jankofsky M, Stilianakis NI, Boedecker RH, Eikmann TF. Effects of bioaerosol polluted outdoor air on airways of residents: a cross sectional study. Occup Environ Med 2003;60:336–42.
[9] Olenchock SA. Health effects of biological agents: the role of endotoxins. Appl Occup Environ Hyg 1994;9(1):62–4.
[10] Castellan RM, Olenchock SA, Kinsley KB, Hankinson JL. Inhaled endotoxin and decreased spirometric values. An exposure-response relation for cotton-dust. New Engl J Med 1987;317:605–10.
[11] Heedrik D, Douwes J. Towards an occupational exposure limit for endotoxins? Ann Agric Environ Med 1997;4:17–9.
[12] Weibel ER. Morphometry of the Human Lung. Berlin: Springer-Verlag; 1963.
[13] Horsfield K, Dart G, Olson DE, Filley GF, Cumming G. Models of the human bronchial tree. J Appl Physiol 1971;31:207–17.
[14] Soong TT, Nicolaides P, Yu CP, Soong SC. A statistical description of the human tracheobronchial tree geometry. Resp Physiol 1979;37:161–72.
[15] Yu CP, Nicolaides P, Soong TT. Effect of random airway sizes on aerosol deposition. Am Ind Hyg Assoc Physiol 1979;40:999–1005.
[16] Koblinger L, Hofmann W. Monte Carlo modeling of aerosol deposition in human lungs. Part I: simulation of particle transport in a stochastic lung structure. J Aerosol Sci 1990;21:661–74.
[17] Koblinger L, Hofmann W. Analysis of human lung morphometric data for stochastic aerosol deposition calculations. Phys Med Biol 1985;30:541–56.
[18] Phillips CG, Kaye SR. On the asymmetry of bifurcations in the bronchial tree. Resp Physiol 1997;107:85–98.
[19] Yeh HC, Schum GM. Models of the human lung airways and their application to inhaled particle deposition. Bull Math Biol 1980;42:461–80.
[20] Carslow HS, Jaeger HC. Conduction of heat in solids. Oxford: Clarendon Press; 1959.
[21] Cohen BS, Asgharian B. Deposition of ultrafine particles in the upper airways. J Aerosol Sci 1990;21:789–97.
[22] Ingham DB. Diffusion of aerosol from a stream flowing through a cylindrical tube. J Aerosol Sci 1975;6:125–32.
[23] Stahlhofen W, Rudolf G, James AC. Intercomparison of experimental regional deposition data. J Aerosol Med 1989;2:285–308.
[24] Cheng KH, Cheng YS, Yeh HC, Guilmette RA, Simpson SQ, Yang Y, et al. *In vivo* measurements of nasal airway dimensions and ultrafine aerosol deposition in the human nasal and oral airways. J Aerosol Sci 1996;27:785–801.

[25] Asgharian B, Yu CP. Deposition of inhaled fibrous particles in the human lung. J Aerosol Med 1988;1:37–50.
[26] Cai FS, Yu CP. Inertial and interceptional deposition of spherical particles and fibers in a bifurcating airway. J Aerosol Sci 1988;19:679–88.
[27] Myojo T, Takaya M. Estimation of fibrous aerosol deposition in upper bronchi based on experimental data with model bifurcation. Ind. Health 2001;39:141–9.
[28] Zhang L, Asgharian B, Anjilvel S. Inertial and interceptional deposition of fibers in abifurcating airway. J Aerosol Med 1996;9:419–30.
[29] Davies CN. Particle–fluid interaction. J Aerosol Sci 1979;10:477–513.
[30] Kasper G. Dynamics and measurement of smokes. I size characterization of nonspherical particles. Aerosol Sci Technol 1982;1:187–99.
[31] Sturm R, Hofmann W. A theoretical approach to the deposition and clearance of fibers with variable size in the human respiratory tract. J Hazard Mater 2009;170:210–21.
[32] International Commission on Radiological Protection (ICRP). Human respiratory tract model for radiological protection, Publication 66. Oxford: Pergamon Press; 1994.
[33] Sturm R. Theoretical approach to the hit probability of lung-cancer-sensitive epithelial cells by mineral fibers with various aspect ratios. Thoracic Cancer 2010;3:116–25.
[34] Sturm R. Deposition and cellular interaction of cancer-inducing particles in the human respiratory tract: theoretical approaches and experimental data. Thoracic Cancer 2010;4:141–52.
[35] Bajc M, Bitzen U, Olsson B, Perez de Sá V, Palmer J, Jonson B. Lung ventilation/perfusion SPECT in the artificially embolized pig. J Nucl Med 2002;43:640–7.
[36] Burch WM, Sullivan PJ, Lomas FE, Evans VA, McLaren CJ, Arnot RN. Lung ventilations studies with Technetium 99 m ''Pseudogas''. J Nucl Med 1986;27:842–6.
[37] Hofmann W, Sturm R. Stochastic model of particle clearance in human bronchial airways. J Aerosol Med 2004;17:73–89.
[38] Burge H. Bioaerosols: prevalence and health effects in the indoor environment. Aller Clin Immunol 1990;86:686–701.